Supporting Information

New Journal of Chemistry

Rare-earth phosphors based on spherical infinite coordination polymers

Guilherme Arroyos, Regina Célia Galvão Frem

São Paulo State University (UNESP), Institute of Chemistry, Araraquara, São Paulo, 14800-970, Brazil

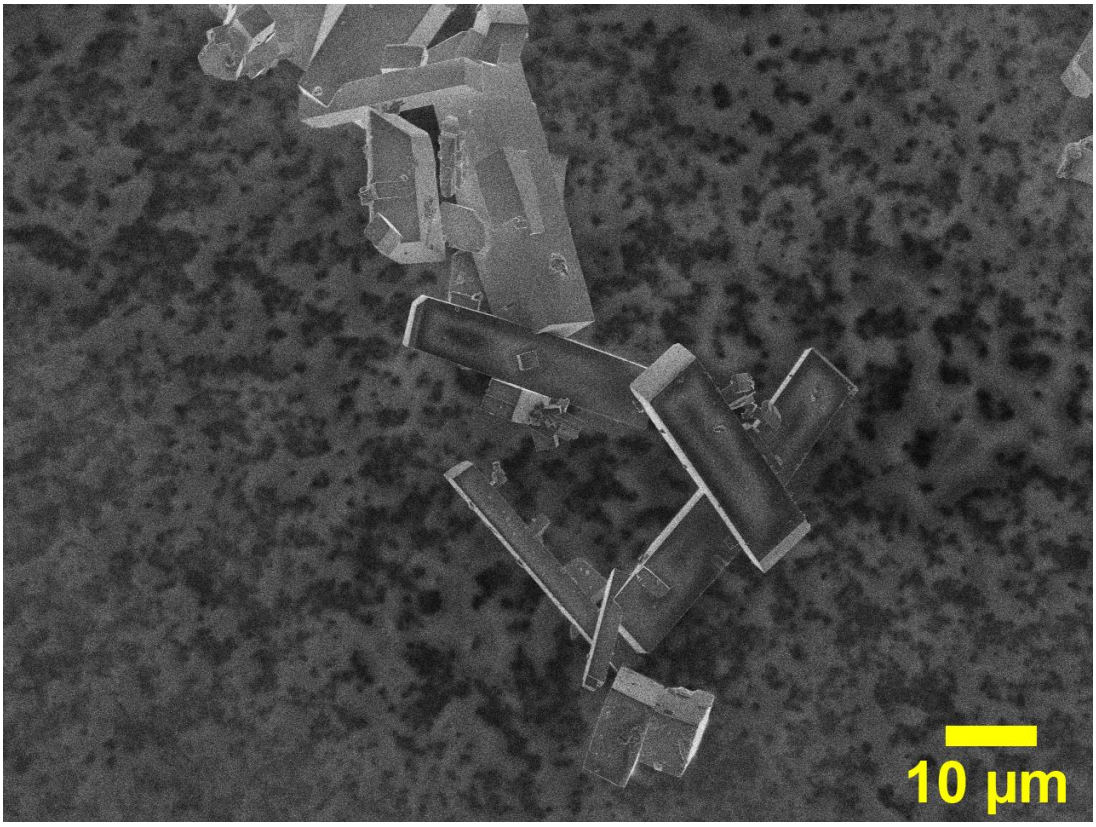

Fig. S1. FEG-SEM image of **Tb-M2** synthesized with pH = 2.

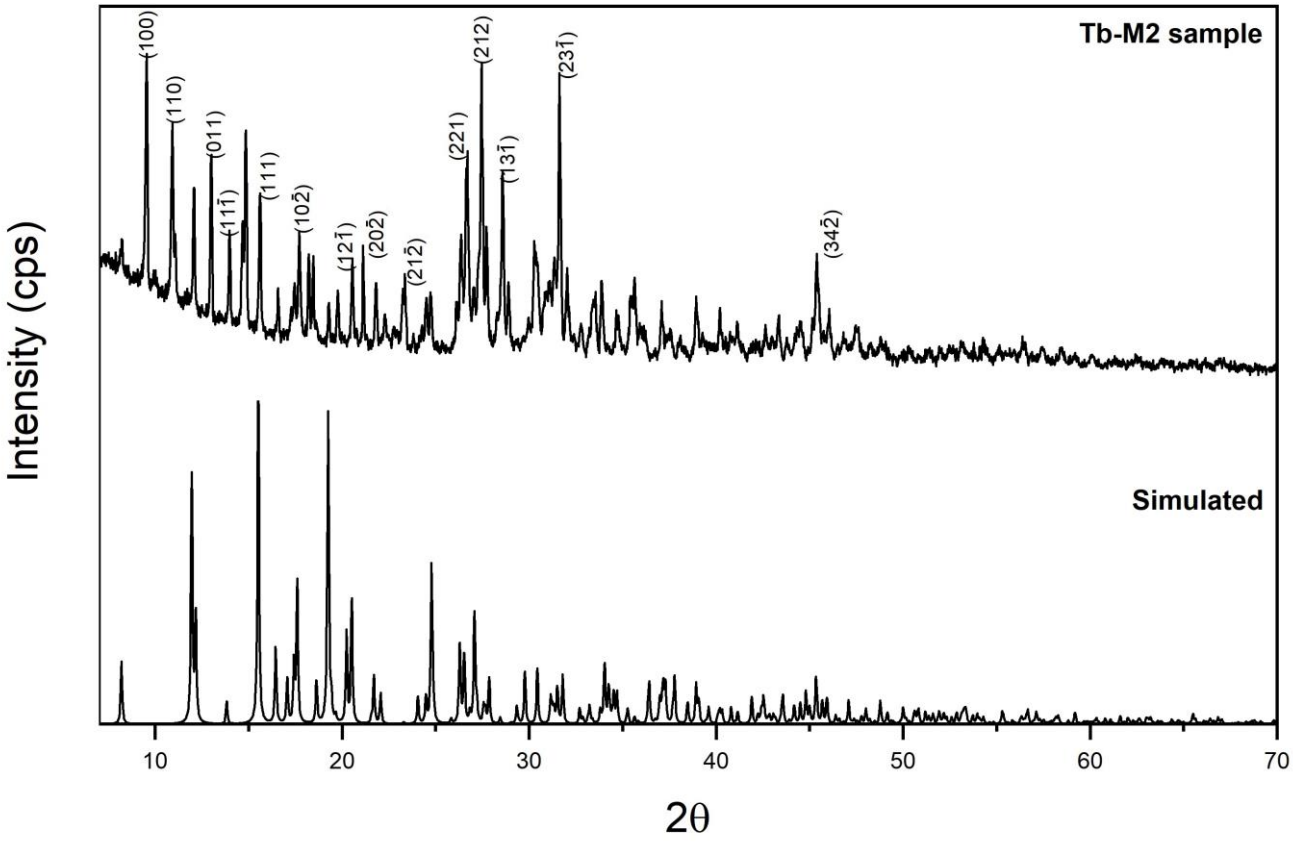

Fig. S2. Powder XRD of **Tb-M2** (top) and simulated data (bottom) ($P2_1/c$, CCDC Deposition Number 614527).

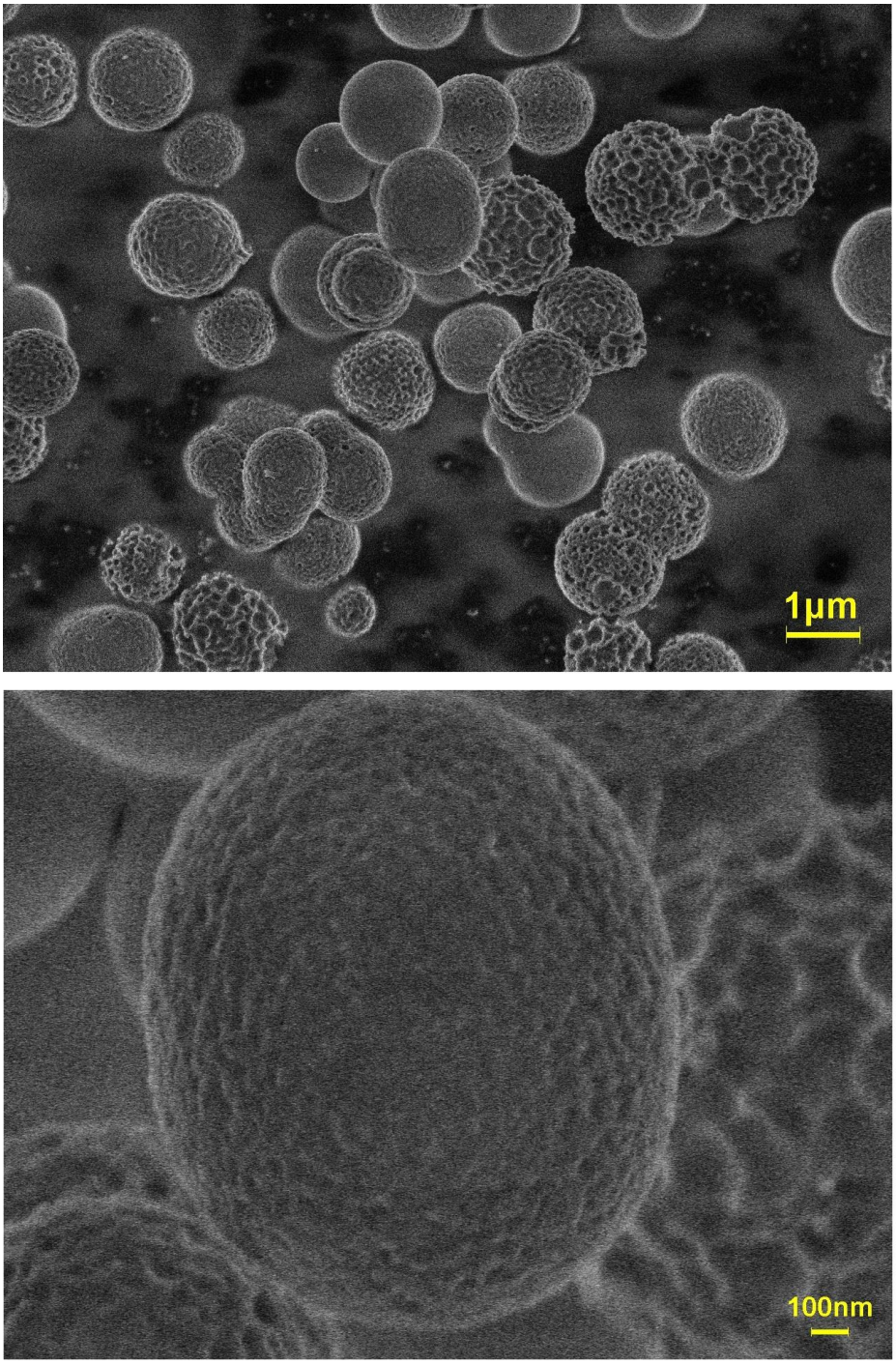

Fig. S3. FEG-SEM images of **Tb-M5** synthesized with pH = 5.

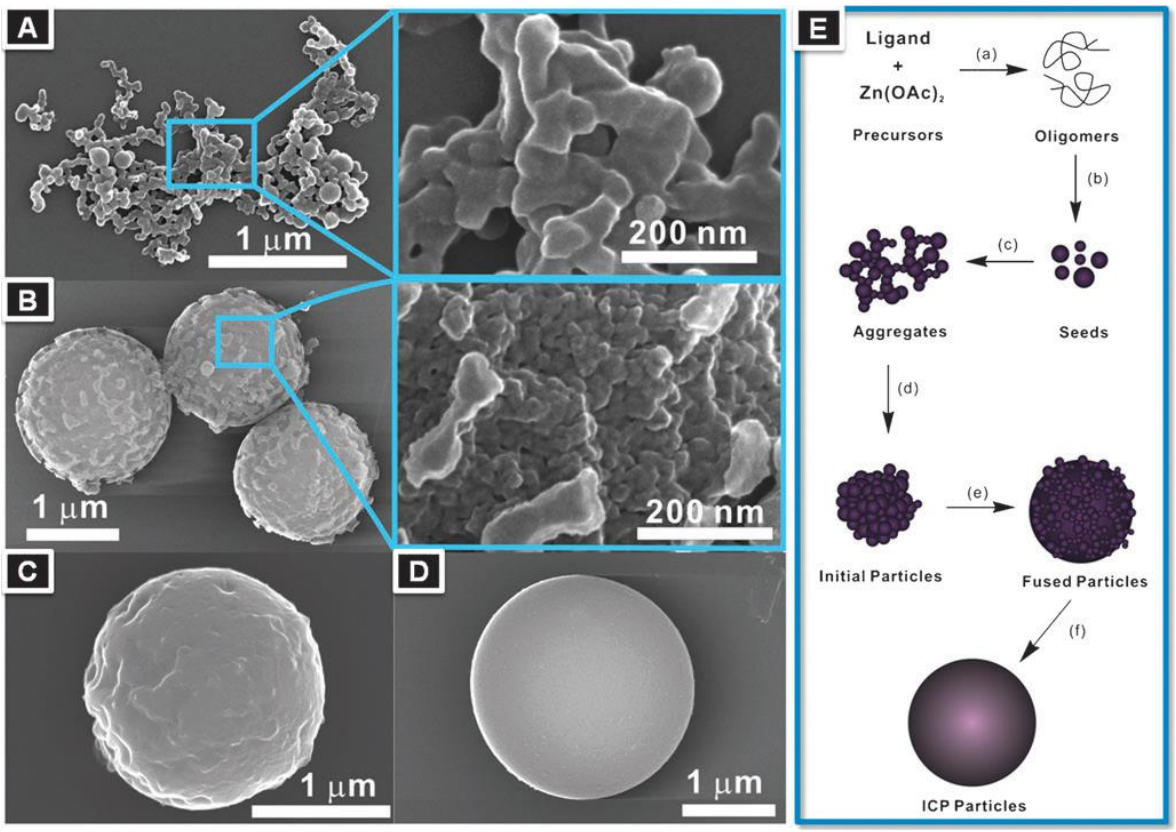

Fig. S4. Proposed mechanism of the formation of the spherical particles for an analogous Zn-based ICP. Reproduced from Ref. 1 with permission from The Royal Society of Chemistry.

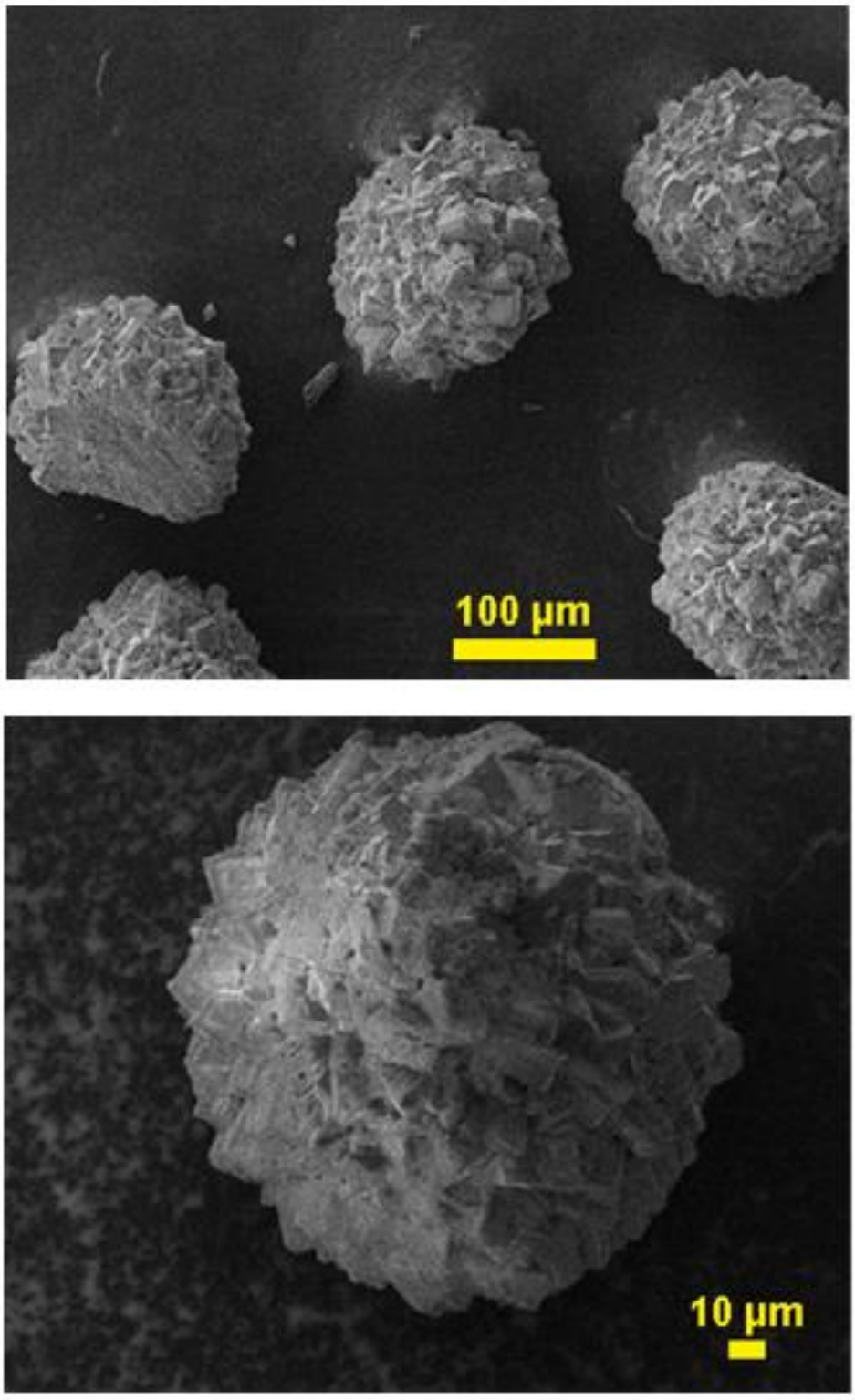

Fig. S5. FEG-SEM images of **Tb-MHT** synthesized with pH = 4.0 by hydrothermal technique, with 72 h at 150 ˚C and 36 h of cooling to room temperature.

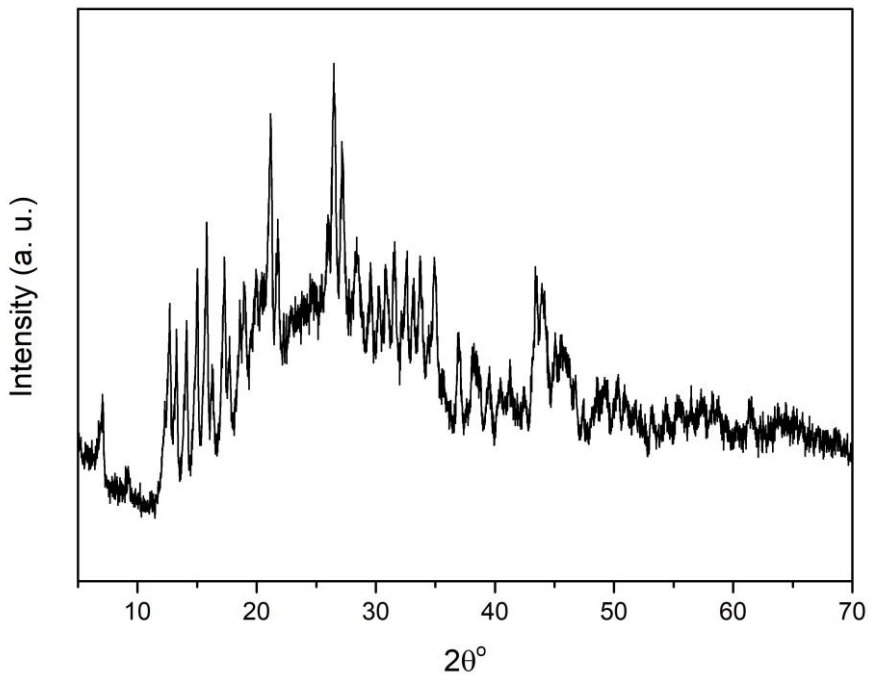

Fig. S6. Powder X-ray diffraction pattern of **Tb-MHT** synthesized with pH = 4.0 by hydrothermal technique, 72 h at 150 ˚C and 36 h of cooling to room temperature.

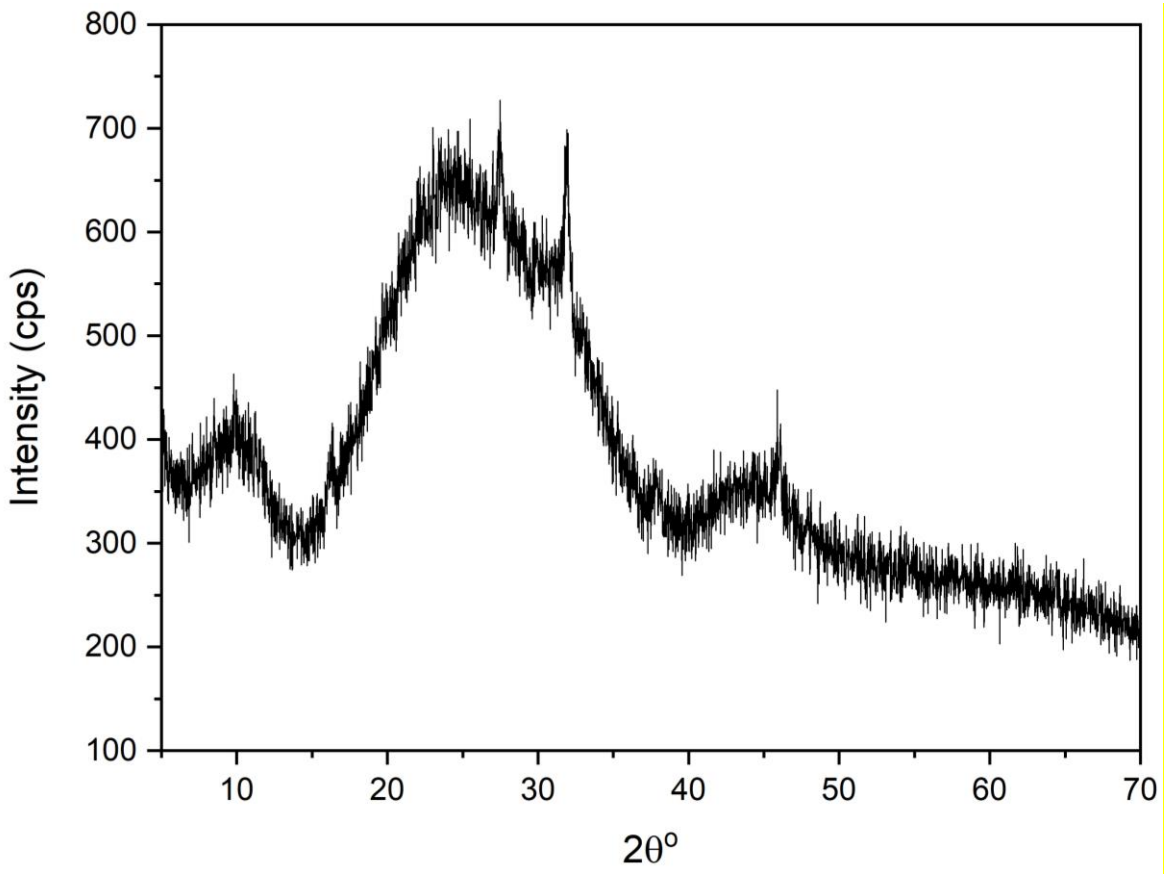

Fig. S7. Powder X-ray diffraction pattern of **Eu-M** compound.

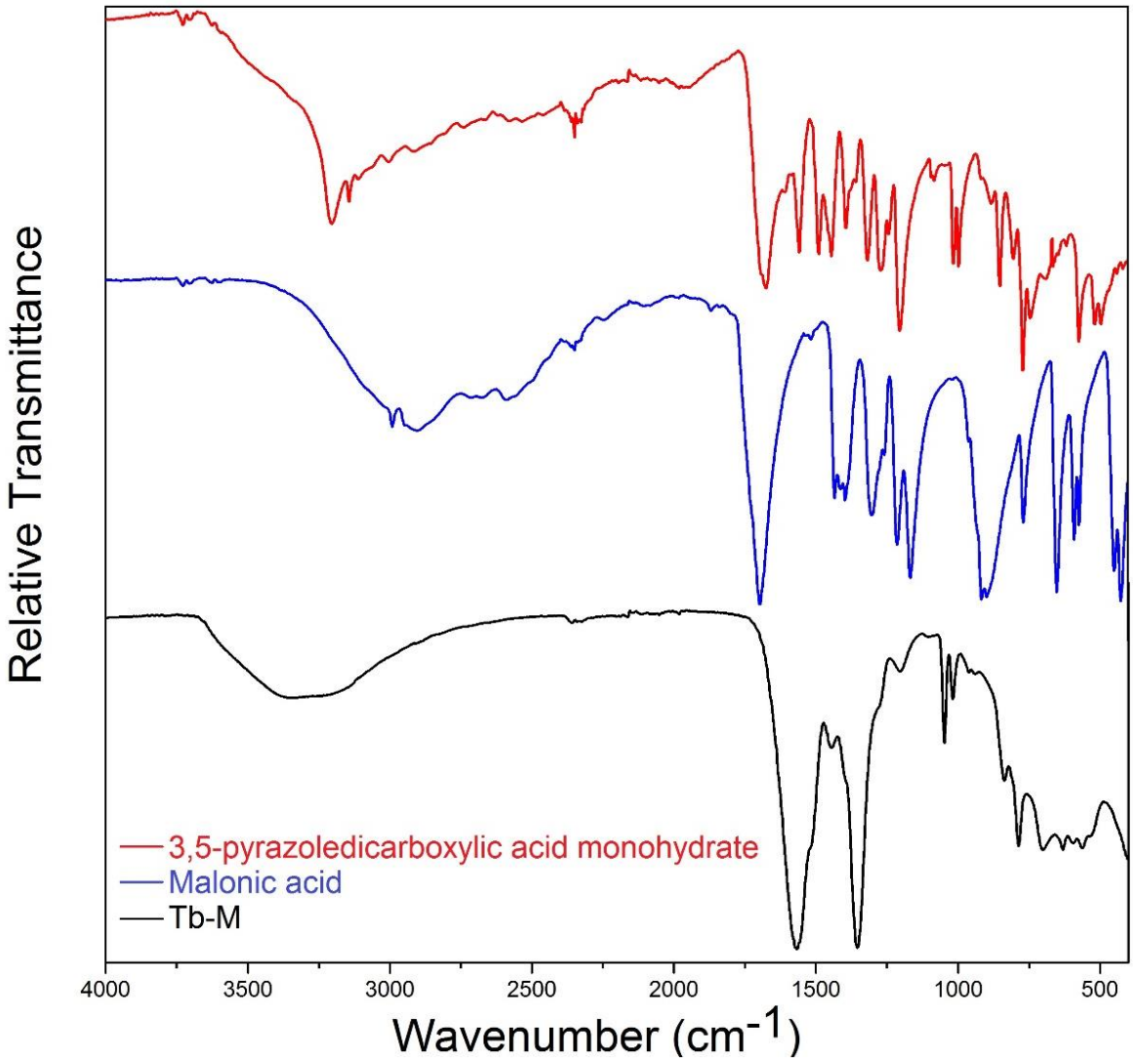

Fig. S8. Infrared spectra of the ligands and **Tb-M**.

Table S1. Main IR vibrational absorption bands and assignments for free ligands and **Tb-M**.

3,5 pyrazoledicarboxylic acid	**Malonic acid**	**Tb-M**	**Assignment**
-	-	3506-3073 *w, br*	ν(OH), ν(NH), ν(CH)
3202 *s, br*	-	-	ν(CH), ν(OH)
3141 *m*	-	-	ν(CH)
3108 *w*	-	-	ν(CH)
3003 *w*	-	-	ν(=CH)
-	2989 *m*	-	ν(OH)
2916 *w*	-	-	ν(CH)
-	2948 *sh*, 2902 *m*	2908 *vw*	ν(CH)
-	-	1565 *vs, br*	ν_{as}(COO)
-	-	1355 *vs, br*	ν_{s}(COO)
-	1697 *vs*	-	ν(C=O), ν(C-O)
1689 *sh*, 1674 *vs*	-	-	ν(C=O)
1557 *s*	-	-	ν_{s}(ring)
1488 *s*	-	-	δ_{ip}(ring)
1442 *s*	-	1444 *w*	ν(ring)
-	1434 *s*	-	δ(CH_2), δ(OH)
1393 *m*	1394 *s*	-	ν(ring), δ(OH), δ(CO), δ(CC)
1314 *s*	-	-	ν(C-O)
-	1301*s*	-	δ(OH), ν(CO_2), ν(CC)
1265 *s*	-	-	δ_{op}(CH)
-	1212 *s*	-	δ_{op}(CH_2)
1206 *vs*		1202 *w, br*	ν_{s}(C=O)
-	1166 *vs*	-	δ_{op}(CH_2)
1014 *s*	-	1017 *w*	δ_{ip}(CH_2), δ_{op}(CH_2), ν(ring)
993 *s*	-	-	δ_{ip}(ring)
-	916 *vs*	-	ν(CC), ν(C-O)
-	897 *vs*	-	δ_{ip}(OH)
853 *s*	-	836 *w*	δ_{op}(CH)
771 *s*	771 *s*	785 *m*	δ_{op}(CH), δ_{ip}(C=O), δ_{ip}(C-O), δ_{ip}(C-C)
746 *m*	-	-	δ_{op}(OH)
-	649 *vs*	630 *w*	δ(CCO)
-	591 *s*	596 *w, br*	δ_{ip}(C=O), δ(CCO)
571 *m*	-	-	δ_{op}(ring)
-	570 *s*	563 *w, br*	δ_{ip}(C=O), δ(CCO)
518 *w*	-	533 *vw*	δ_{op}(NH)
496 *w*	-	-	δ(OCO)
-	448 *vs*	-	δ_{ip}(CCO)
-	427 *vs*	-	δ_{ip}(CCO)

ν: stretching; ν_s: symmetrical stretching; ν_{as}: asymmetrical stretching; δ_{op}: out-of-plane deformation; δ_{ip}: in-plane deformation.

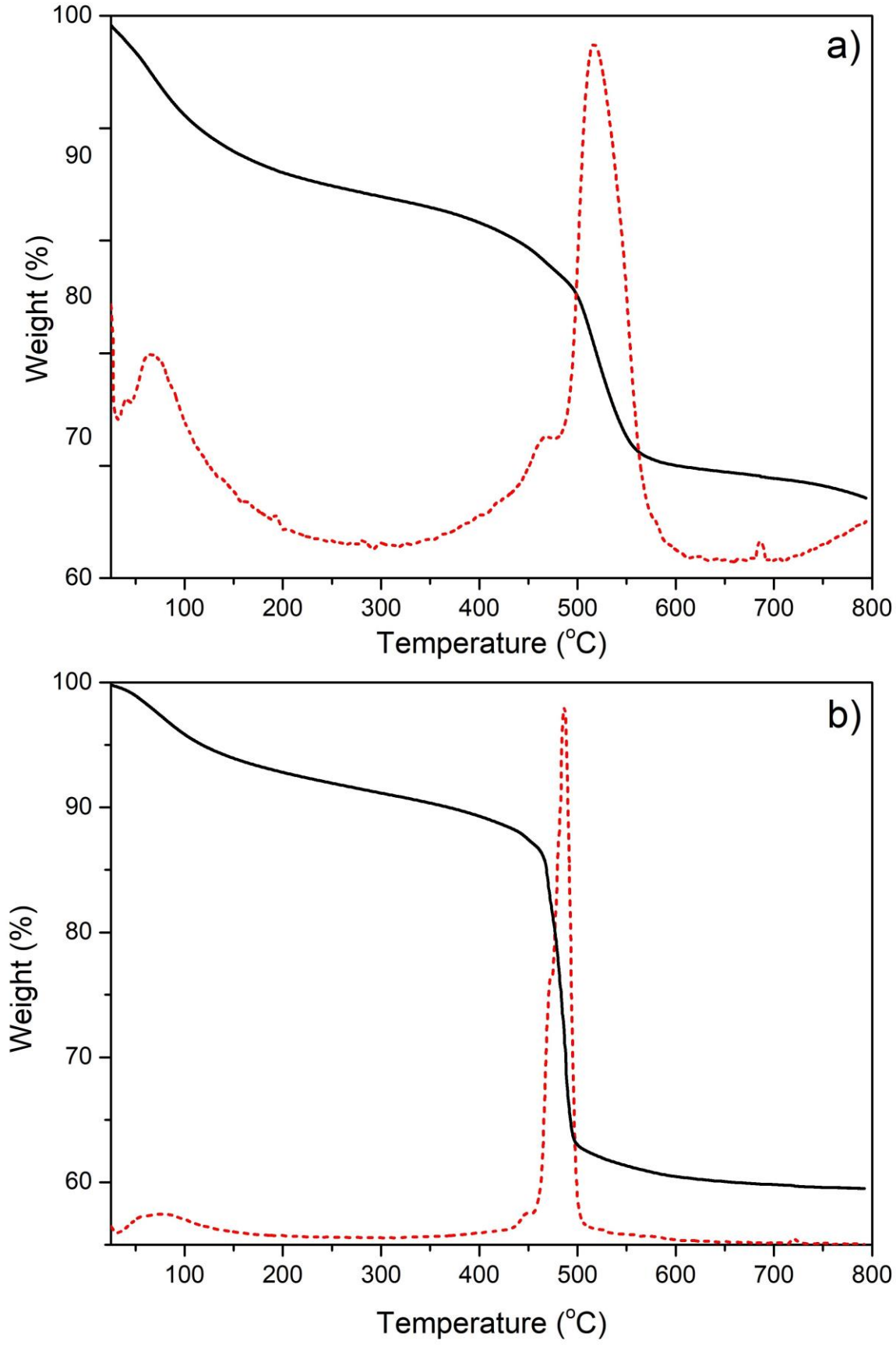

Fig. S9. TG/DTG curves of as-synthesized **Tb-M** (a) and after activation (b).

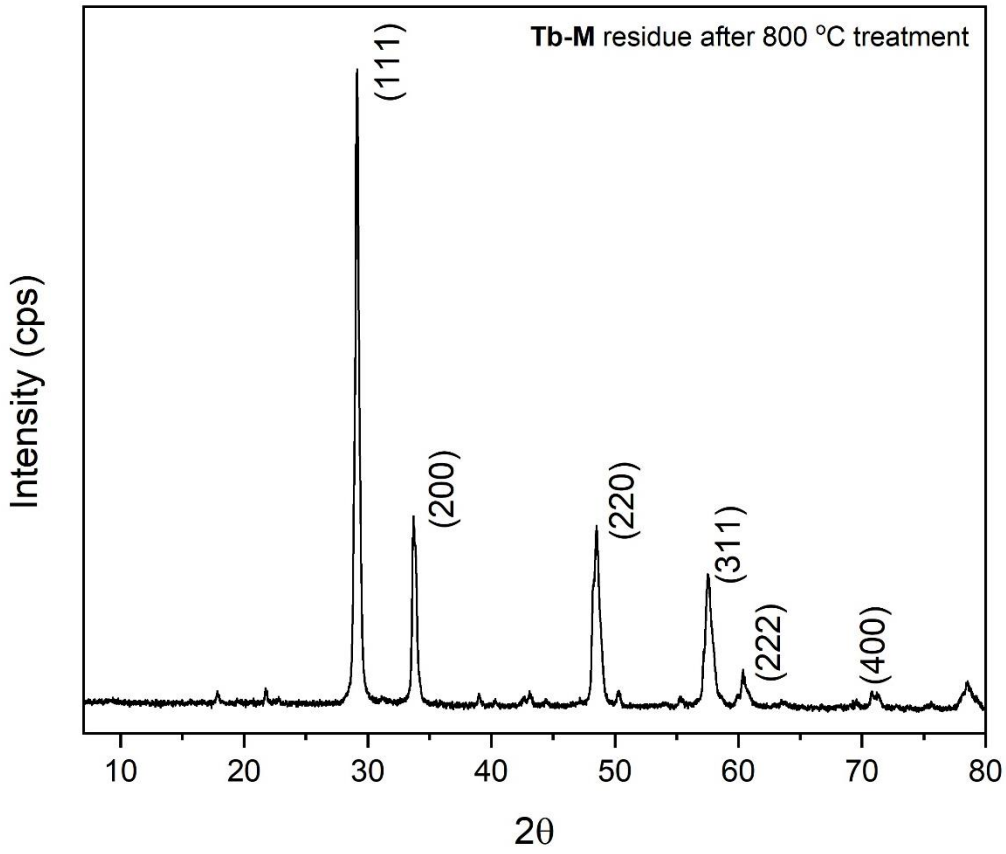

Fig. S10. XRD pattern of **Tb-M** residue after 800 ºC treatment showing Tb_4O_7 characteristic peaks.

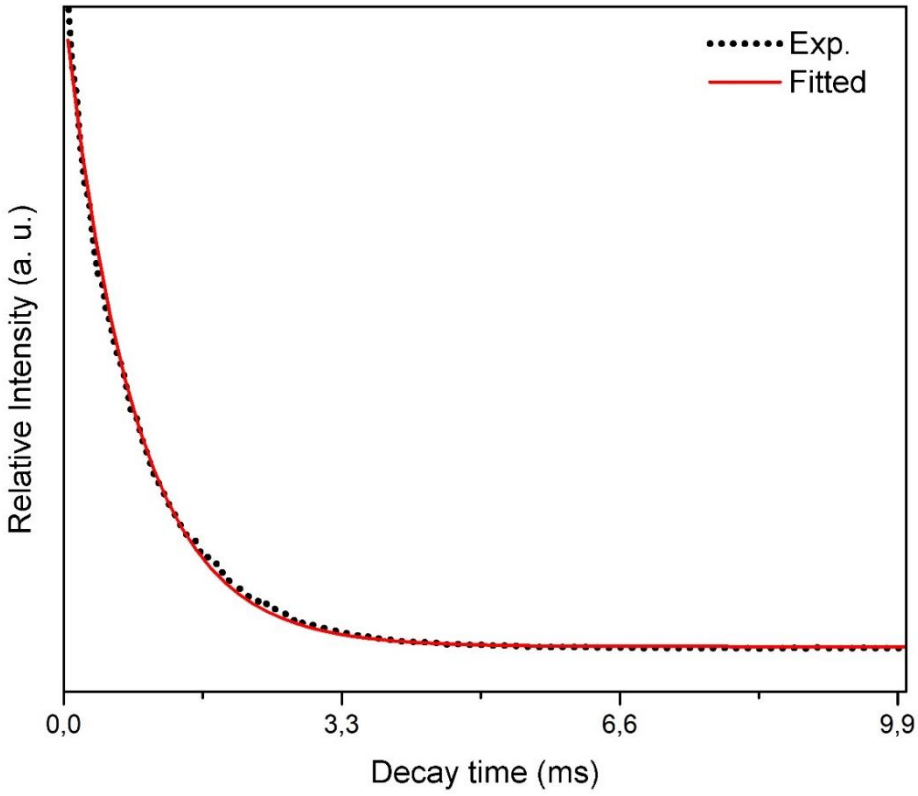

Fig. S11. Decay time curves of **Tb-M**.

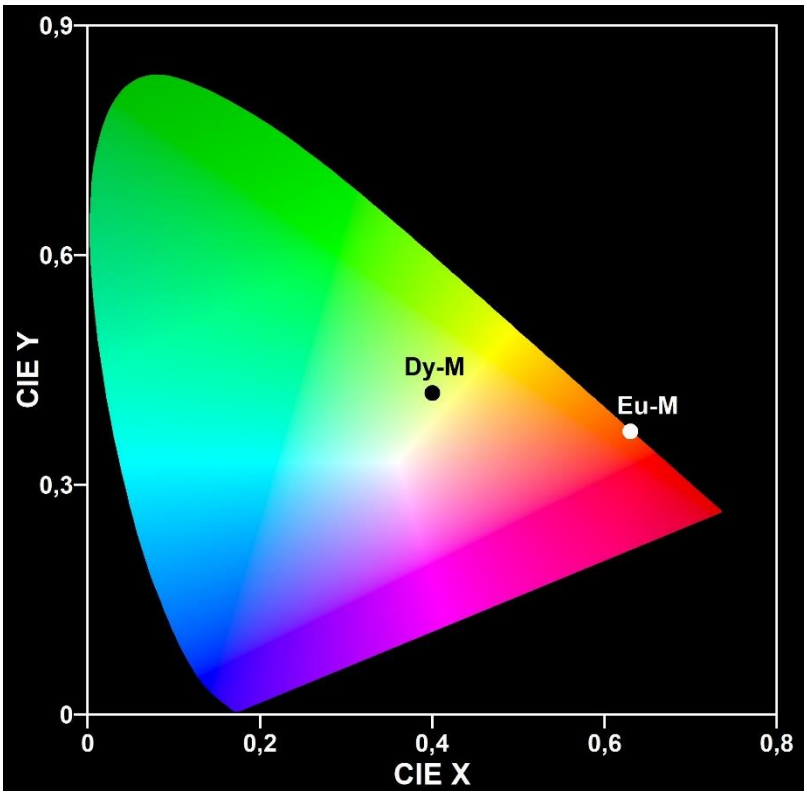

Fig. S12. CIE chromaticity diagram for **Eu-M** (0.63, 0.37) and **Dy-M** (0.40, 0.42) samples.

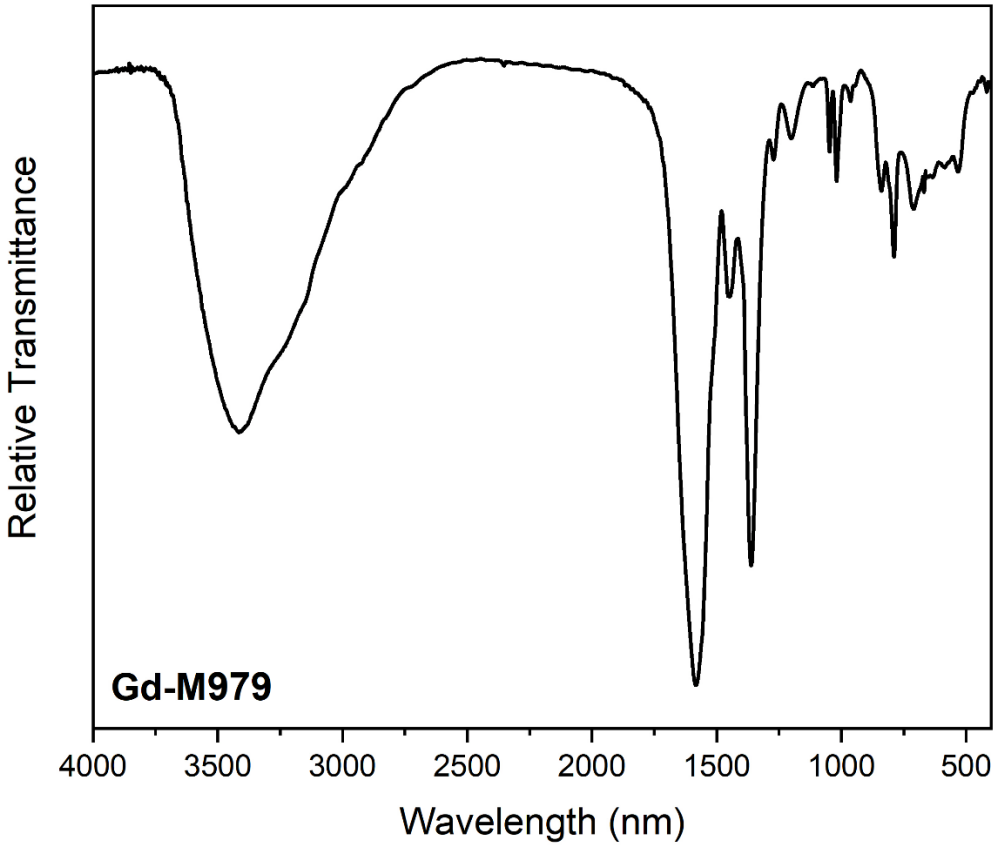

Fig. S13. Infrared spectrum of **Gd-M979**.

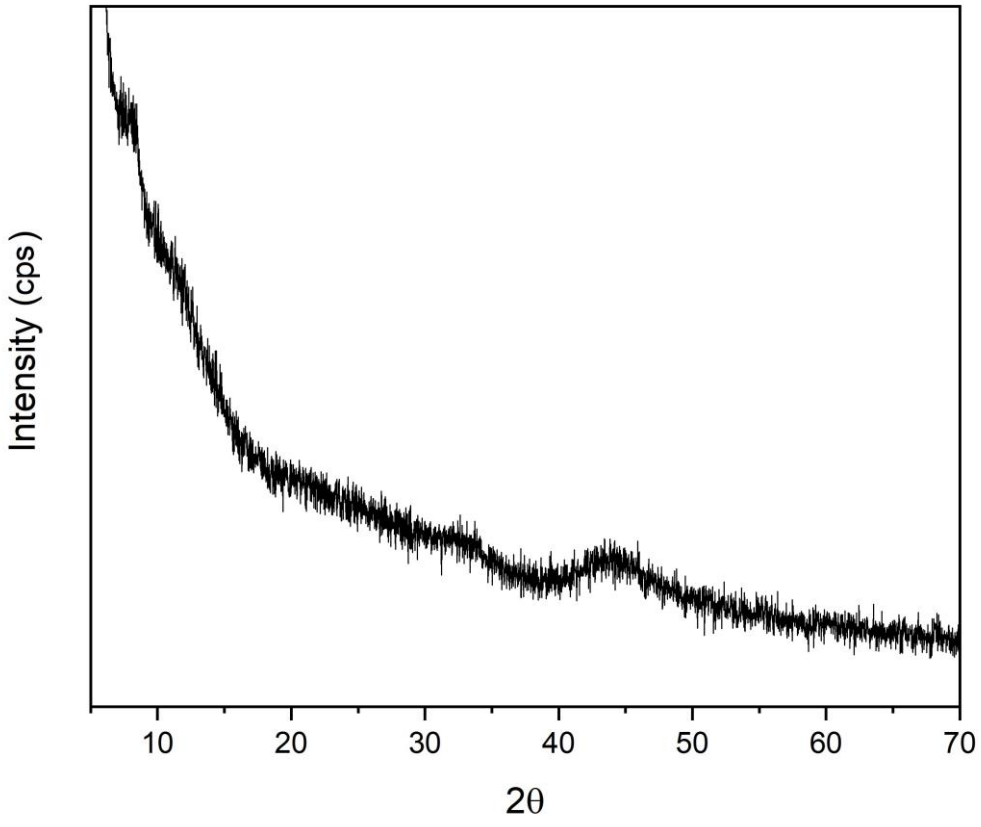

Fig. S14. Powder X-ray diffraction pattern of **Gd-M979**.